Micro focusing of fast electrons with opened cone targets

Feng Liu, Xiaoxuan Liu, Bicheng Liu, Wenjun Ding, Fei Du et al.

Citation: Phys. Plasmas **19**, 013103 (2012); doi: 10.1063/1.3671954
View online: http://dx.doi.org/10.1063/1.3671954
View Table of Contents: http://pop.aip.org/resource/1/PHPAEN/v19/i1
Published by the American Institute of Physics.

Micro focusing of fast electrons with opened cone targets

Feng Liu (刘峰),[1] Xiaoxuan Liu (林晓宣),[1] Bicheng Liu (刘必成),[1,2] Wenjun Ding (丁文君),[1] Fei Du (杜飞),[1] Yutong Li (李玉同),[1,a)] Jinglong Ma (马景龙),[1] Xiaolong Liu (刘晓龙),[1] Zhengming Sheng (盛政明),[1,3] Liming Chen (陈黎明),[1] Xin Lu (鲁欣),[1] Quanli Dong (董全力),[1] Weimin Wang (王伟民),[1] Zhaohua Wang (王兆华),[1] Zhiyi Wei (魏志义),[1] and Jie Zhang (张杰)[1,3,a)]
[1]*Institute of Physics, Chinese Academy of Sciences, Beijing 100190, China*
[2]*State Key Laboratory of Nuclear Physics and Technology, Institute of Heavy Ion Physics, Peking University, Beijing 100871, China*
[3]*Department of Physics, Shanghai Jiao Tong University, Shanghai 200240, China*

(Received 20 June 2011; accepted 7 November 2011; published online 6 January 2012)

Using opened reentrant cone silicon targets, we have demonstrated the effect of micro focusing of fast electrons generated in intense laser-plasma interactions. When an intense femtosecond laser pulse is focused tightly onto one of the side walls of the cone, fast electron beam emitted along the side wall is observed. When a line focus spot, which is long enough to irradiate both of the side walls of the cone simultaneously, is used, two electron beams emitted along each side wall, respectively, are observed. The two beams should cross each other near the open tip of the cone, resulting in micro focusing. We use a two-dimensional Particle-In-Cell code to simulate the electron emission both in opened and closed cone targets. The simulation results of the opened cone targets are in agreement with the experimental observation while the results of the closed cone targets do not show the micro focusing effect. © *2012 American Institute of Physics*. [doi:10.1063/1.3671954]

I. INTRODUCTION

The generation and transport of fast electrons during the interactions of high intensity short laser pulses with solid targets are critical for the applications such as the x-ray generation,[1] high magnitude magnetic field generation[2] and the ion acceleration,[3] particularly fast ignition scenario for laser confinement fusion.[4] Recently, behaviors of fast electrons in a solid cone target are studied both in experiments[5] and simulations[6] because the cone target can shield the corona plasma and guide the heating short pulse laser into high density region of the pre-compressed plasma.[7] Some of the results indicated that the side walls of the cone target could also guide the fast electrons to the tip of the cone,[8] which is very helpful in the triggering of the fusion pellet[9] or the acceleration of the ions.[10] However, some experiments, in which Kα imaging technique was used to measure the fast electron transport in a conical target sealed by a plane solid foil, did not indicate the guiding effect of the fast electrons because no obvious enhancement of the Kα emission was observed.[11] For the sealed conical targets, connecting the tip of the cone with the plane foil with glue may affect the fast electron transport,[12] and it is difficult to distinguish the electrons generated at the side walls from the electrons at the tip.

In order to study the guiding effect of the conical targets, we have diagnosed the spatial distribution of the fast electrons emitted from an opened cone targets without any sealed foils at the tip. With the opened cone targets, we can distinguish the electrons generated at the walls from those generated at the tip because there is no apparent solid density plasma at the tip of the cone. The spatial distributions clearly show that two distinct electron beams corresponding to each side of the conical wall are generated when the two side walls are irradiated by the laser pulses simultaneously. This indicates that under appropriate conditions the fast electrons from the side walls are focused toward the open tip of the cone. We find that the number of the forward fast electrons can be highly enhanced by using different focus conditions in the opened cone. We have carried out two-dimensional (2D) particle-in-cell (PIC) simulations of the opened cone targets. The results agree with the experimental measurements. For comparison, we also utilize common closed cone targets in the simulations.[13–16] We find that the spontaneous magnetic and electric fields at the sealed plane foil behind the tip will change the behavior of the fast electrons when they exit the cone tip, resulting in no micro focusing effect.

II. EXPERIMENT SETUP

The experiment was carried out using the Extreme Light II (XL II) femtosecond laser system[17] at the Institute of Physics, Chinese Academy of Sciences. The laser was p-polarized and operated at 800 nm with pulse duration of about 60 fs and energy of 300 mJ in the experiment. The laser pulses were focused into the opened cone targets with an f/3.5, 90°off axis parabolic mirror. Far-field measurements gave a 5 μm (FWHM) diameter laser spot with a corresponding peak intensity of 6×10^{18} W/cm^2. Third order autocorrelation measurement revealed the presence of a short 10^{-6} pre-pulse arriving 10 ps before the main pulse. Such kind of pre-pulse produced pre-plasma after impinging the targets.

The opened cone targets used in the experiment were manufactured from ⟨100⟩ single crystal silicon wafers by

a)Authors to whom correspondence should be addressed. Electronic mail: ytli@aphy.iphy.ac.cn or jzhang1@sjtu.edu.cn.

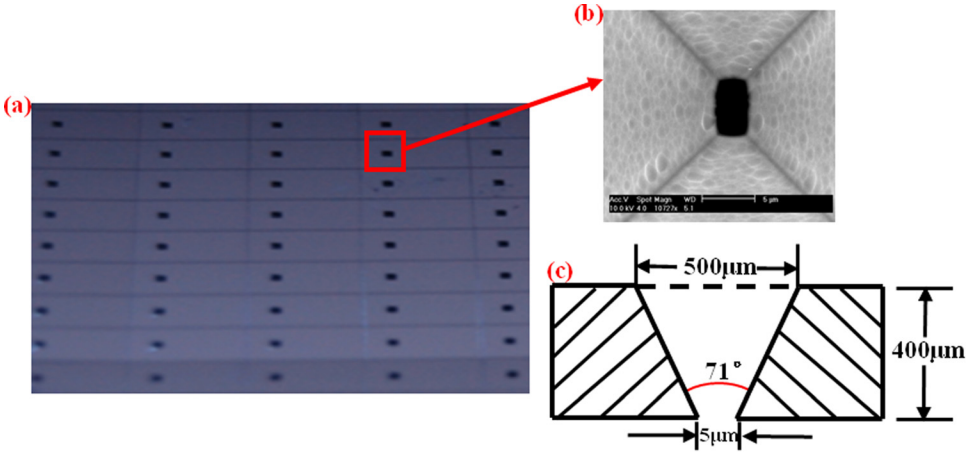

FIG. 1. (Color online) (a) Image of the re-entrant cone arrays etched in a silicon wafer. (b) Image of an etched cone taken by a scanning electron microscope (top view). (c) Schematic view of the cone configuration. The width of the open entrance is 5 μm.

means of standard semiconductor processing techniques.[18] When the wafer is etched in KOH solution, along the $\langle 111 \rangle$ direction, the etching rate is faster than $\langle 100 \rangle$. With suitable masks and etching time we can produce four-side cone targets with the size of the opened-tip 5 μm and opening angle 71°. The arrays and configuration of the targets are shown in Fig. 1. The sharpness of the edge of the cone tip is guaranteed by the precision of the photo-etching mask. For 400-μm-thick silicon wafers and opening squares 500×500 μm^2, tip sharpness is better than 1×1 μm^2. This is important for the similarity between the real cones used in the integrated fast ignition experiments[19] and our experimental ones. Figure 1(c) illustrates that the schematic structure of the opened cone targets.

One of the technological difficulties when using such kind of micro-structured targets is the alignment of the target and the incident laser.[20] Since the cone targets are opened, we tackle this by observing the forward leak laser directly with an objective lens and a CCD. When the target is precisely aligned with the incident laser, the leak image has a symmetric distribution on the CCD. By carefully adjusting the target and the laser, the 5 μm laser focal spot was aligned into the opening tip of the target with a 1 μm precision.

In the vacuum target chamber, three layers of imaging plates (IPs)[21] (type: BAS-SR2040) separated by 13 μm aluminum filters between each layer then wrapped by a 13 μm aluminum filter were placed 50 mm behind the cone target to measure the fast electrons escaped from the target. The front aluminum filters were used to block the visible light and the separated aluminum filters are intended to select different electron energies. When we used a pair of magnets in front of the imaging plate no obvious signal was found, which indicated that the signal on the imaging plate mainly came from electrons. The imaging plates covered about 140° in horizontal direction and about 100° in vertical direction. The setup is schematically shown in Fig. 2.

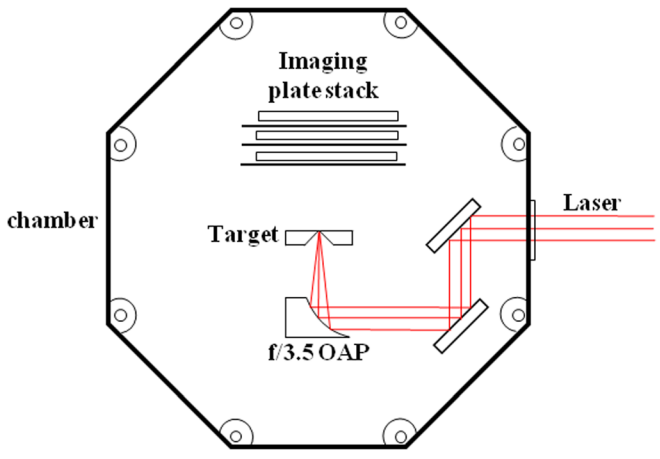

FIG. 2. (Color online) Schematic picture of the experimental setup. The IP stack behind the target detects the spatial distributions of the fast electrons.

In the experiment, using the microscopically imaging system we controlled the focal spot to interact with the cone target in three cases, as shown in the left column of Fig. 3, (i) the laser pulse was tightly focused and aligned with the symmetrical axis of the cone target; (ii) the laser pulse was tightly focused onto one of the side walls and its axis paralleled with the axis of the cone; (iii) the laser pulse was adjusted to be a line focus and interacted with two side walls simultaneously, while paralleling with the axis of the cone. In this case, the laser light is also p-polarized and the size of the line focus spot is 20 μm long and 5 μm high. With the similar laser energy and pulse duration as the case (i) and case (ii), the laser irradiance is 1.5×10^{18} W/cm^2 on target.

We also plan to carry out an experiment by using femtosecond laser interaction with closed cone targets. However, this experiment was not made due to large reflection of laser light from the target.

III. EXPERIMENTAL RESULTS

The measured electron spatial distributions for the three focusing cases are shown in Figs. 3(a)-3(i). Because of the stopping effect of the imaging plates and the aluminum filters, each layer of the imaging plates detects different energy intervals of the electrons. The minimum detected energy of each layer is calculated by the code CASINO.[22]

In case (i), the fast electrons are mainly emitted in the direction of the laser propagation, as shown in Figs. 3(a)–3(c). The diameter of the laser spot (FWHM) is comparable to the opened width of the target. Therefore, most of the laser energy cannot directly interact with the walls but with the pre-plasma generated by the ASE and pre-pulse. The beam pattern on the first layer is more like a disk with a divergence angle of 69°. On the second layer, the divergence

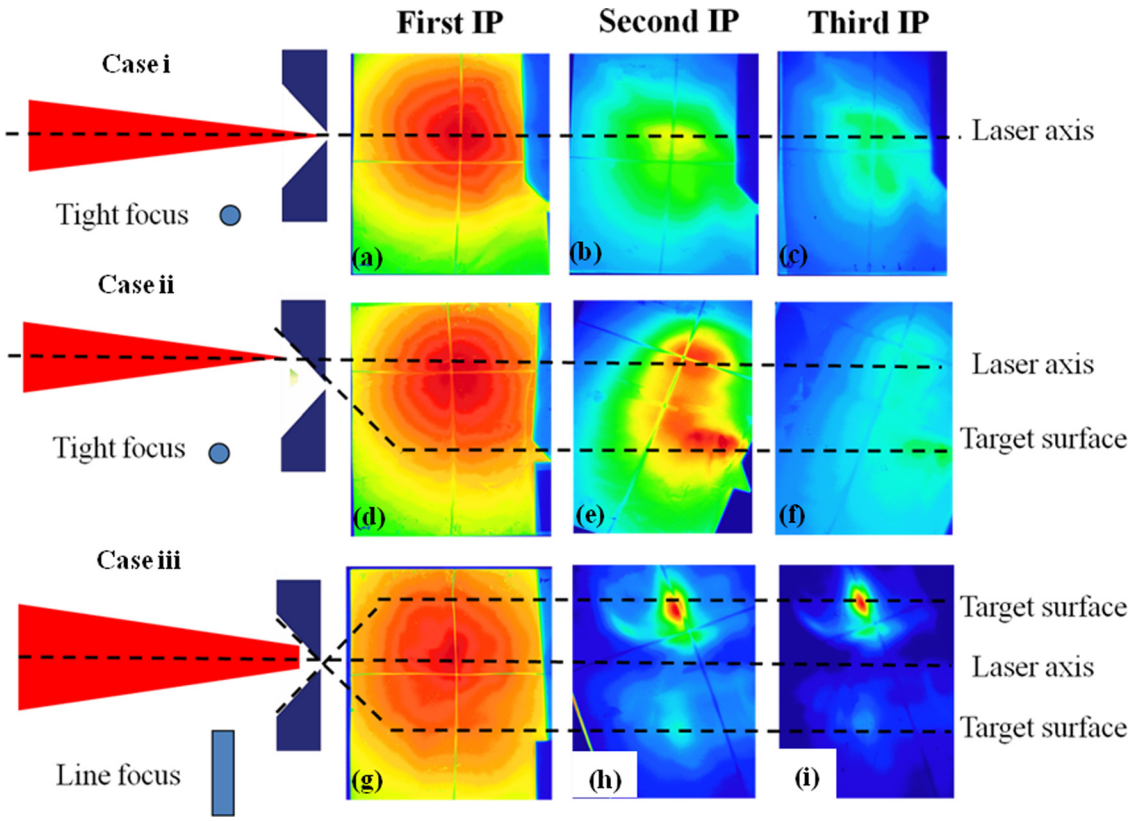

FIG. 3. (Color online) Typical fast electron spatial distributions detected by imaging plates behind the opened cone target. The focusing and target geometry are illustrated on the left. Each column of the images has the same detected energy interval and is scaled to the same intensity level. The first layer of the imaging plates detects the fast electrons with energies >45 keV, the second layer > 550 keV, and the third layer >900 keV, respectively.

is reduced to 41° and on the third layer 34°. The electrons are believed to be generated by the ponderomotive force, which accelerates the electrons in the forward laser propagation direction.[23]

In case (ii), the spatial distribution of the electrons with lower energy (first layer) is similar to the case (i). However, for the higher energy electrons (second and third layer), another bunch of electrons in addition to the electrons in the laser propagation direction is presented [Figs. 3(e) and 3(f)]. This new electron bunch is emitted in the direction of the side wall, onto which the laser pulse is shined. In the first layer, the signal of this electron bunch is covered by the lower energy electron component. This indicates that the electrons in the direction of the wall have higher energy and fewer numbers. We believe that this bunch of electrons is generated due to the quasi-static electric and magnetic field generated by the interaction of the laser with the wall as discussed below.

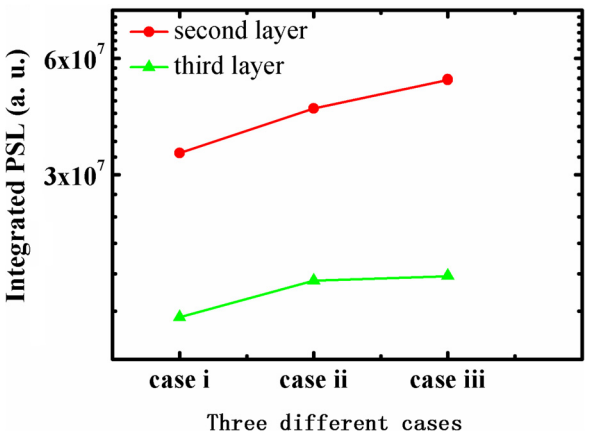

FIG. 4. (Color online) The integrated intensity of the signal on the three IP layers for three cases. Cases (i), (ii), and (iii) correspond to the three cases described in the text.

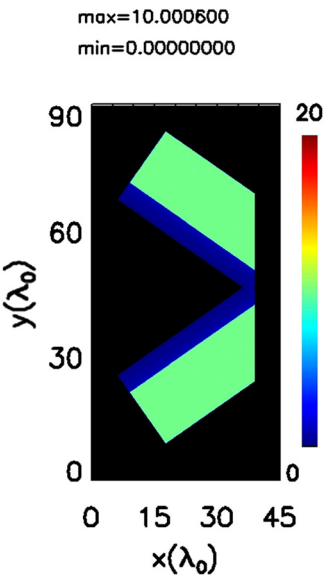

FIG. 5. (Color online) The 2D PIC simulation configuration of the interactions.

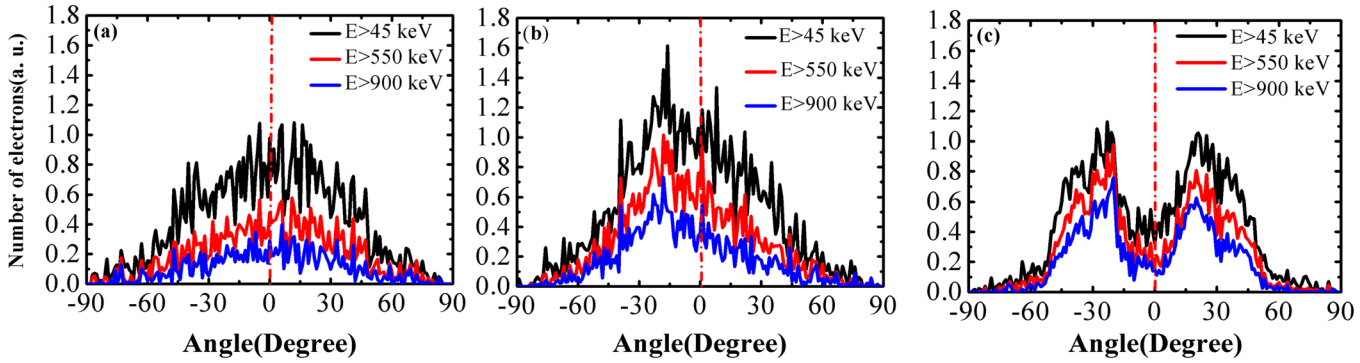

FIG. 6. (Color online) (a) The simulated angular distributions of the fast electrons out of the entrance of the cone targets for case (i), (b) case (ii), and (c) case (iii) at time t=906 fs. The red dashed dotted line indicates the laser propagation direction (0°).

In case (iii) the line laser spot interacts with the two opposite walls of the cone target. The angular distribution of the electrons with lower energy is similar to the other two cases. However, for the electrons with higher energy, it is clearly seen that two distinct regions of electron signals are observed, as shown in Figs. 3(h) and 3(i). These two bunches of electrons lie in the direction of the two side walls. These two bunches of fast electrons should cross each other out of the entrance of the cone resulting in micro focusing.

Figure 4 shows the integrated electron signal on the second and third layer of the imaging plates. For the three cases, the incident laser energy is almost kept to be similar. The signal intensity of case (ii) is stronger than that of case (i). The signal intensity of case (iii) is stronger than the other two cases. Those indicate that more electrons are generated and transported to the tip of the cone when the laser interacted with the walls of the cone target. Note that for case (iii) the laser intensity is lower than the other two cases since the area of the line focus is larger while the laser energies are similar.

IV. SIMULATIONS AND DISCUSSIONS

In order to understand the fast electron emission, we have carried out 2D particle-in-cell simulations with a relativistic fully electromagnetic code.[24] The configuration of the simulations is illustrated in Fig. 5. The simulation box is $45\lambda_0 \times 90\lambda_0$, where λ_0=0.8 μm is the central wavelength of the incident laser light in vacuum. There are 25 cells per wavelength and 25 particles per cell. The opened cone target is composed of two plasma slabs, each of which is $35\lambda_0$ long, $15\lambda_0$ wide with a density $10n_c$, where n_c is the critical density. The two plasma slabs are separated by a distance $5\lambda_0$ to simulate the opened entrance of the cone targets. Each of the plasma slabs is covered by a pre-plasma with a density $0.1n_c$ and a scale length $2\lambda_0$. The laser is incident from the left.

The simulations of the interactions are also classified by the laser spot shape and position as illustrated in the left column of Fig. 3. We changed the laser focus spot both in the position and shape while keeping the target the same during the simulation to coincide with the experiment. We diagnosed the fast electrons angular distribution out of the entrance of the opened target. The simulated angular distributions of the fast electrons are plotted in Fig. 6, in which 0° corresponds to the symmetrical axis of the target.

In Fig. 6(a), we can see that the when the laser pulse was focused tightly along the symmetric axis of the cone, fast electrons are emitted mainly in the direction of the cone axis for all energy intervals, which are similar to the pattern observed in the experiment. Figure 6(b) shows that when the laser pulse was tightly focused onto one of the side walls, the distribution peak of fast electrons is shifted to the direction of the cone wall. However, a large number of fast electrons are still emitted in the laser direction. In Fig. 6(c), two peaks are presented in the directions of the two side walls. This pattern is similar to the experimental result in case (iii). We have used several different scale lengths of the pre-plasma to see how the pre-plasma affects the fast electron generation and transport. We find the two peaks will not dominate the distribution if the scale of the pre-plasma is too large or small in case (iii). Figure 7(a) shows the simulated angular distribution of the fast electrons with a pre-plasma scale

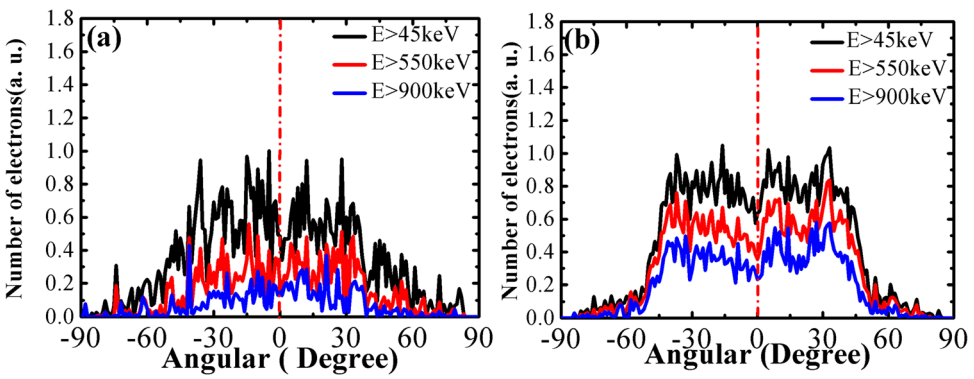

FIG. 7. (Color online) The simulated angular distribution of the fast electrons in case (iii) with a pre-plasma scale length (a) $0.1\lambda_0$ (b) $6\lambda_0$.

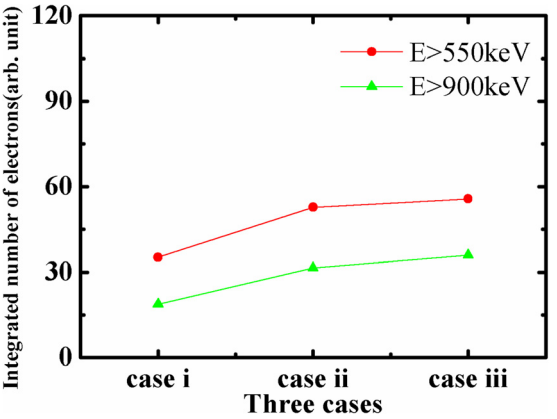

FIG. 8. (Color online) The integrated intensity of fast electrons in different energy intervals for the opened cone targets.

length $0.1\lambda_0$. In this result the two peaks disappeared, which is probably because that under such circumstances the absorption rate of the incident pulse laser on the side walls will decrease and the total number of fast electrons along the surface of the side walls is reduced. Figure 7(b) demonstrates the angular distribution of the fast electrons with a pre-plasma scale length $6\lambda_0$ and the contrast ratio of the two peaks to the base of the distribution is substantially decreased, which results from the destruction of the quasi-static magnetic and electric field in pre-plasma with large scale length.

Figure 8 shows the integrated intensity of the simulated fast electrons with energies $E > 550$ keV and $E > 900$ keV for the three cases. We can see that the change of the integrated numbers of fast electrons is similar to the experimental results, where more electrons are accelerated along the side wall of the opened cone target in case (iii).

The surface magnetic fields are very crucial to the generation of the fast electrons along the surface of the target wall. The time-average magnetic field distributions for all three cases at the time of 240 fs are shown in Fig. 9. The magnetic field is normalized to $\omega_0 m_e/e$, where e is the electron charge, ω_0 is the frequency of the incident laser wave in vacuum, m_e is the mass of the electron. We can see that the magnetic field distributions for the three cases are different. In case (i), because of the tight focus the main laser pulse cannot interact with the cone walls, the magnetic field at the surface of the inner walls does not grow up. In the other two cases strong magnetic fields are generated at the inner surfaces of the cone wall.[25] Because of the quasi-static magnetic fields, the fast electrons flow along the cone wall. We also diagnose the time averaged current density in case (ii) and case (iii), as shown in Fig. 10. The current density is normalized to ecn_c, where c is the speed of light in vacuum. The current density along the cone wall in the region of the interaction can be clearly distinguished from the background.

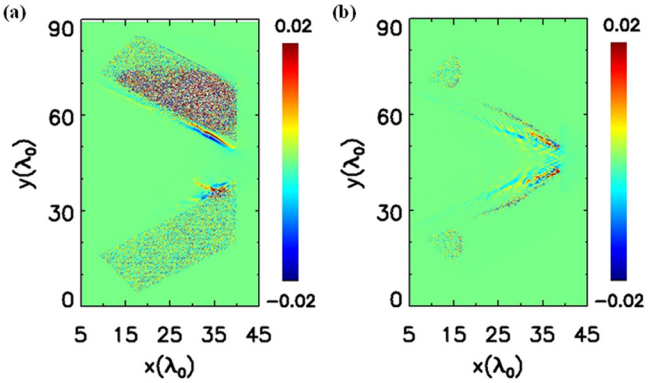

FIG. 10. (Color online) (a) The time-averaged current density for case (ii) and (b) case (iii) at time t=240 fs.

In order to compare with the opened cone targets we carry out another simulation by using closed cone targets. We construct the target by adding a plane plasma slab with a thickness of $6\lambda_0$just behind the tip of the cone (see Fig. 11). The laser is incident into the cone from the left as a line focus. The laser intensity is the same as the simulation in case (iii) with opened cone targets. The angular distributions of the fast electrons with different energies for the closed target are shown in Fig. 12. We can see that the angular distributions just have one peak presented in the direction of the incident laser. This is much different with the result shown in Fig. 6(c).

Figure 13 shows the distributions of the static magnetic fields, electric fields, and the current densities in closed-tip cone at two times t=160 fs and t=187 fs. It is implied that the collision effect in the slab and the quasi-static magnetic and the static electric fields change the transportation of the fast electrons and smear the two peaks into one peak only. Also the solid state plasma just in front of the laser will be heated and resulting in more electrons accelerated in the laser direction. In the opened cone targets case, there is no apparent solid state plasma and no sharp boundary between plasma and vacuum at the tip, where the magnetic field is

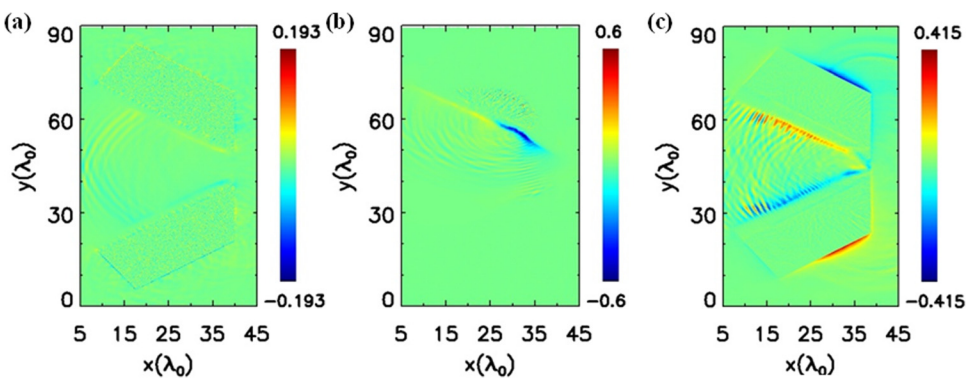

FIG. 9. (Color online) (a) The time-averaged magnetic field distributions for case (i), (b) case (ii), and (c) case (iii) at time t=240 fs.

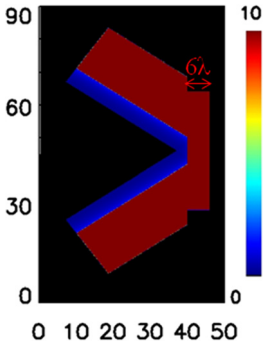

FIG. 11. (Color online) The density map of the closed cone targets with a plane slab thickness $6\lambda_0$ behind the opened cone. There is no gap between the slab and the cone. The laser is incident from the left.

small, as shown in Fig. 9(c). The electrons can escape easily from the cone keeping their initial status at the side walls.

V. CONCLUSION

The spatial distributions of the fast electrons emitted from the tip of the opened micro cone targets when irradiated by femtosecond laser pulses for different laser focus conditions have been investigated. In line focus case, the spatial distribution of the electrons with energy more than 550 keV are emitted mainly in the direction of the side wall and the integrated signal intensity is enhanced compared to the other two cases, which means that more electrons flow into the tip of the cone. We attribute this micro focusing to the quasi-static magnetic field when the laser pulse interacts with the side walls of the cone. We also compare the angular distributions of the emitted fast electrons from both opened and closed targets by simulations. For closed cone targets, there is no apparent micro-focusing effect. Fast electron micro focusing with cone targets is favorable to the ignition of the inertial confinement fusion, the x-ray generation, and the acceleration of the ions. Moreover, such targets may be used as a kind of plasma device to control the behavior of the fast electrons during the interaction of the short pulse laser with solid state targets.

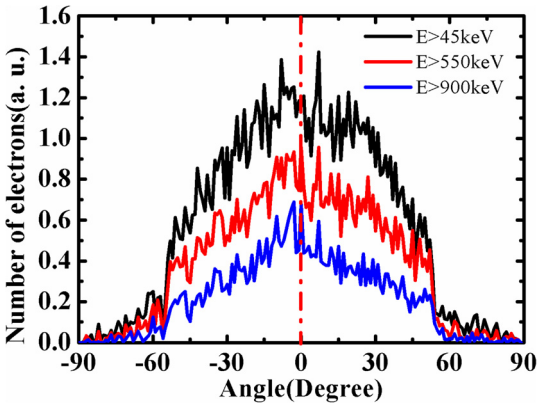

FIG. 12. (Color online) The simulated angular distributions of the fast electrons emitted from the closed cone targets when the laser is incident into the cone as a line focus. The red dashed dotted line indicates the laser propagation direction (0°).

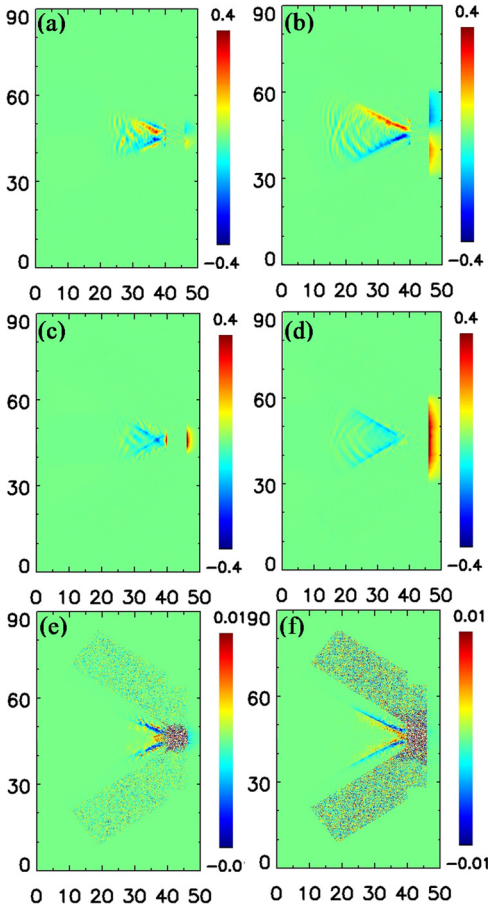

FIG. 13. (Color online) (a) The distributions of the static magnetic field B_z for the sealed cone target at time t=160 fs and (b) at t=187 fs. (c) The distributions of the static electric field E_x at time t=160 fs and (d) at t=187 fs. (e) The distributions of the current density j_x at time t=160 fs and (f) at t=187 fs.

ACKNOWLEDGMENTS

This work is supported by the National Nature Science Foundation of China (Grant Nos. 10925421, 10735050, 10734130, 10935002).

[1]L. M. Chen, M. Kando, M. H. Xu, Y. T. Li, J. Koga, M. Chen, H. Xu, X. H. Yuan, Q. L. Dong, Z. M. Sheng, S. V. Bulanov, Y. Kato, J. Zhang, and T. Tajima, Phys. Rev. Lett. **100**, 045004 (2008).
[2]H. B. Cai, W. Yu, S. P. Zhu, and C. T. Zhou, Phys. Rev. E **76**, 036403 (2007).
[3]S. C. Wilks, A. B. Langdon, T. E. Cowan, M. Roth, M. Singh, S. Hatchett, M. H. Key, D. Pennington, A. MacKinnon, and R. A. Snavely, Phys. Plasmas **8**, 542 (2001).
[4]M. Tabak, J. Hammer, M. E. Glinsky, W. L. Kruer, S. C. Wilks, J. Woodworth, E. M. Campbell, M. D. Perry, and R. J. Mason, Phys. Plasmas **1**, 1626 (1994).
[5]B. I. Cho, G. M. Dyer, S. Kneip, S. Pikuz, D. R. Symes, A. C. Bernstein, Y. Sentoku, N. R. L. Galloudec, T. E. Cowan, and T. Ditmire, Phys. Plasmas **15**, 052701 (2008).
[6]Y. Sentoku, K. Mima, H. Ruhl, Y. Toyama, R. Kodama, and T. E. Cowan, Phys. Plasmas **11**, 3083 (2004).
[7]R. Kodama, P. A. Norreys, K. Mima, A. E. Dangor, R. G. Evans, H. Fujita, Y. Kitagawa, K. Krushelnick, T. Miyakoshi, N. Miyanaga, T. Norimatsu, S. J. Rose, T. Shozaki, K. Shigemori, A. Sunahara, M. Tampo, K. A. Tanaka, Y. Toyama, T. Yamanaka, and M. Zepf, Nature (London) **412**, 798 (2001).
[8]Y. T. Li, X. H. Yuan, M. H. Xu, Z. Y. Zheng, Z. M. Sheng, M. Chen, Y. Y. Ma, W. X. Liang, Q. Z. Yu, Y. Zhang, F. Liu, Z. H. Wang, Z. Y. Wei, W. Zhao, Z. Jin, and J. Zhang, Phys. Rev. Lett. **96**, 165003 (2006);

X. H. Yuan, Y. T. Li, M. H. Xu, Z. Y. Zheng, Q. Z. Yu, W. X. Liang, Y. Zhang, F. Liu, J. Bernhardt, S. J. Wang, Z. H. Wang, W. J. Ling, Z. Y. Wei, W. Zhao, and J. Zhang, Opt. Express **16**, 81 (2008).
[9]R. Kodama, H. Azechi, H. Fujita, H. Habara, Y. Izawa, T. Jitsuno, T. Jozaki, Y. Kitagawa, K. Krushelnick, T. Matsuoka, K. Mima, N. Miyanaga, K. Nagai, H. Nagatomo, M. Nakai, H. Nishimura, T. Norimatsu, P. Norreys, K. Shigemori, H. Shiraga, A. Sunahara, K. A. Tanaka, M. Tanpo, Y. Toyama, K. Tsubakimoto, T. Yamanaka, and M. Zepf, Nucl. Fusion **44**, S276 (2004).
[10]K. A. Flippo, E. d'Humières, S. A. Gaillard, J. Rassuchine, D. C. Gautier, M. Schollmeier, F. Nurnberg, J. L. Kline, J. Adams, B. Albright, M. Bakeman, K. Harres, R. P. Johnson, G. Korgan, S. Letzring, S. Malekos, N. Renard-LeGalloudec, Y. Sentoku, T. Shimada, M. Roth, T. E. Cowan, J. C. Fernández, and B. M. Hegelich, Phys. Plasmas **15**, 056709 (2008).
[11]S. D. Baton, M. Koenig, J. Fuchs, A. Benuzzi-Mounaix, P. Guillou, B. Loupias, T. Vinci, L. Gremillet, C. Rousseaux, M. Drouin, E. Lefebvre, F. Dorchies, C. Fourment, J. J. Santos, D. Batani, A. Morace, R. Redaelli, M. Nakatsutsumi, R. Kodama, A. Nishida, N. Ozaki, T. Norimatsu, Y. Aglitskiy, S. Atzeni, and A. Schiavi, Phys. Plasmas **15**, 042706 (2008).
[12]L. Van Woerkom, K. U. Akli, T. Bartal, F. N. Beg, S. Chawla, C. D. Chen, E. Chowdhury, R. R. Freeman, D. Hey, M. H. Key, J. A. King, A. Link, T. Ma, A. J. MacKinnon, A. G. MacPhee, D. Offermann, V. Ovchinnikov, P. K. Patel, D. W. Schumacher, R. B. Stephens, and Y. Y. Tsui, Phys. Plasmas **15**, 056304 (2008).
[13]K. A. Tanaka, R. Kodama, K. Mima, Y. Kitagawa, H. Fujita, N. Miyanaga, K. Nagai, T. Norimatsu, T. Sato, Y. Sentoku, K. Shigemori, A. Sunahara, T. Shozaki, M. Tanpo, S. Tohyama, T. Yabuuchi, J. Zheng, T. Yamanaka, P. A. Norreys, R. Evanse, M. Zepf, K. Krushelnic, A. Dangor, R. Stephens, S. Hatchett, M. Tabak, and R. Turner, Phys. Plasmas **10**, 1925 (2003).
[14]Z. L. Chen, R. Kodama, M. Nakatsutsumi, H. Nakamura, M. Tampo, K. A. Tanaka, Y. Toyama, T. Tsutsumi, and T. Yabuuchi, Phys. Rev. E **71**, 036403 (2005).
[15]T. Nakamura, H. Sakagami, T. Johzaki, H. Nagatomo, K. Mima, and J. Koga, Phys. Plasmas **14**, 103105 (2007).
[16]B. Chisman, Y. Sentuku, and A. J. Kemp, Phys. Plasmas **15**, 056309 (2008).
[17]J. Zhang, M. Suzuki, M. Baba, Z. Y. Wei, Z. H. Wang, P. Wang, J. A. Zheng, and H. Kuroda, Appl. Opt. **46**, 2498 (2007).
[18]K. Sato, M. Shikida, Y. Matsushima, T. Yamashiro, K. Asaumi, Y. Iriye, and M. Yamamoto, Sens. Actuators, A **64**, 87 (1998).
[19]R. Kodama, H. Shiraga, K. Shigemori, Y. Toyama, S. Fujioka, H. Azechi, H. Fujita, H. Habara, T. Hall, Y. Izawa, T. Jitsuno, Y. Kitagawa, K. M. Krushelnick, K. L. Lancaster, K. Mima, K. Nagai, M. Nakai, H. Nishimura, T. Norimatsu, P. A. Norreys, S. Sakabe, K. A. Tanaka, A. Youssef, M. Zepf, and T. Yamanaka, Nature (London) **418**, 933 (2002).
[20]N. R. L. Galloudec, B. I. Cho, J. Osterholz, and T. Ditmire, Rev. Sci. Instrum. **79**, 083506 (2008).
[21]K. A. Tanaka, T. Yabuuchi, T. Sato, R. Kodama, Y. Kitagawa, T. Takahashi, T. Ikeda, Y. Honda, and S. Okuda, Rev. Sci. Instrum. **76**, 013507 (2005).
[22]D. Drouin, A. R. Couture, D. Joly, X. Tastet, V. Aimez, and R. Gauvin, Scanning **29**, 92 (2007).
[23]S. C. Wilks, W. L. Kruer, M. Tabak, and A. B. Langdon, Phys. Rev. Lett. **69**, 1383 (1992); G. Malka and J. L. Miquel, Phys. Rev. Lett. **77**, 75 (1996).
[24]W. J. Ding, Z. M. Sheng, J. Zhang, and M. Y. Yu, Phys. Plasmas **16**, 042315 (2009).
[25]T. Nakamura, S. Kato, H. Nagatomo, and K. Mima, Phys. Rev. Lett. **93**, 265002 (2004); M. Chen, Z. M. Sheng, J. Zheng, Y. Y. Ma, M. A. Bari, Y. T. Li, and J. Zhang, Opt. Express **14**, 3093 (2006).